Structure and gating mechanism of the acetylcholine receptor pore

Atsuo Miyazawa*, **Yoshinori Fujiyoshi**† & **Nigel Unwin**‡

* RIKEN Harima Institute, 1-1-1 Kouto, Mikazuki-cho, Sayo, Hyogo 679-5148, Japan
† Department of Biophysics, Faculty of Science, Kyoto University, Oiwake, Kitashirakawa, Sakyo-ku, Kyoto 606-8502, Japan
‡ MRC Laboratory of Molecular Biology, Hills Road, Cambridge CB2 2QH, UK

....

The nicotinic acetylcholine receptor controls electrical signalling between nerve and muscle cells by opening and closing a gated, membrane-spanning pore. Here we present an atomic model of the closed pore, obtained by electron microscopy of crystalline postsynaptic membranes. The pore is shaped by an inner ring of 5 α-helices, which curve radially to create a tapering path for the ions, and an outer ring of 15 α-helices, which coil around each other and shield the inner ring from the lipids. The gate is a constricting hydrophobic girdle at the middle of the lipid bilayer, formed by weak interactions between neighbouring inner helices. When acetylcholine enters the ligand-binding domain, it triggers rotations of the protein chains on opposite sides of the entrance to the pore. These rotations are communicated through the inner helices, and open the pore by breaking the girdle apart.

The propagation of electrical signals between nerve cells and their targets takes place at the chemical synapse through the action of transmitter-gated ion channels. These fast-acting molecular switches are oligomeric proteins composed of two main functional parts: an extracellular, ligand-binding domain, and a gated, membrane-spanning pore. Neurotransmitter released from the nerve terminal enters the ligand-binding domain on the surface of the target cell, and triggers a transient conformational change that opens the gate in the membrane-spanning pore. Ions then flow selectively through the pore down their electrochemical gradients, giving rise to a change in membrane potential.

The acetylcholine (ACh) receptor, at the nerve–muscle synapse, is a member of a superfamily of transmitter-gated ion channels, which includes the serotonin 5-HT$_3$, γ-aminobutyric-acid (GABA$_A$ and GABA$_C$) and glycine receptors[1]. It has a cation-selective pore, delineated by a ring of five subunits (α, α, β, γ or ε, δ), that opens upon binding of ACh to distant sites in the two α-subunits at or near the subunit interfaces[2–4]. There are four predicted membrane-spanning segments, M1–M4, in each subunit. The second membrane-spanning segment, M2, shapes the lumen of the pore, and forms the gate of the closed channel. Although much information has been obtained about the roles of individual amino acids in affecting ion transport, and about their relative positions on the membrane-spanning segments, their detailed three-dimensional arrangement has not yet been visualized in this receptor, or in any other transmitter-gated ion channel. Nor is it known how the ACh-triggered conformational change is communicated through the membrane to open the pore.

The (muscle-derived) electric organ of the *Torpedo* electric ray is highly enriched in ACh-receptor-containing membranes, and has been a valuable source of tissue for physiological and biochemical studies of neurotransmission for more than 50 years. The isolated postsynaptic membranes are also amenable to structure analysis by electron microscopy. They convert readily into tubular crystals, having receptors and intervening lipid molecules organized like they are *in vivo*[5,6] (Fig. 1), and enable different functional conformations to be investigated under near-physiological ionic conditions. A description of the amino-terminal ligand-binding domain of the receptor has been obtained by fitting the β-sheet core structure from a homologous pentameric ACh-binding protein, AChBP[7], to the three-dimensional densities determined from electron images[8]. However, the quality of these images and distortions of the crystal lattice limited previous descriptions of the pore, revealing some

α-helical folding, but only in the pore-lining segments[9]. By recording exceptional images at liquid-helium temperatures[10] and applying a computational method to correct for the distortions[11], we have now extended the resolution to 4 Å. We report here an atomic model of the pore domain based on the 4-Å density map, and propose an explanation of how the pore opens when ACh binds to the receptor.

Structure determination

Tubular crystals, having helical symmetry, were grown from *Torpedo marmorata* membranes, and imaged in thin films of amorphous ice (see Methods). Altogether 359 images (~10^6 receptors), involving four helical families, were analysed.

The tubes were too small to yield accurate amplitudes by electron diffraction, so the amplitude, as well as the phase terms, had to be measured from Fourier transforms of the images, and then added vectorially to enhance the signal-to-noise ratio. The amplitudes showed resolution-dependent fading, which was compensated by scaling the measured values against values calculated from a model

Figure 1 Cross-section of a tubular crystal, at low resolution. The receptor protein projects from either side of the membrane, visible as two concentric rings of density, 30 Å apart. A single receptor, cut centrally, is shown at the top. The membrane-spanning pore and the N-terminal ligand-binding domain, shaping a large central vestibule, are outlined by red and green rectangles, respectively. The surfaces encompassing the hydrophobic core of the membrane are assumed to lie along the centres of the rings of density[48].

 949

Table 1 **Image data**

	Helical family				Combined
	(−16,6)	(−17,5)	(−15,7)	(−18,6)	
Tube diameter (Å)	770	760	788	832	
Number of images	160	77	72	50	359
Number of receptors	4.8×10^5	2.2×10^5	2.3×10^5	1.4×10^5	1.1×10^6
Mean defocus (μm; ±s.d.)	1.28 ± 0.29	1.27 ± 0.17	1.32 ± 0.19	1.32 ± 0.25	
Segment length (Å; ±s.d.)	683 ± 52	685 ± 54	676 ± 53	674 ± 49	
Number of layer-lines	1,092	1,065	1,057	1,041	
Independent Fourier terms	1.12×10^5	1.08×10^5	1.04×10^5	1.06×10^5	
Phase errors (degrees)*					
> 9.5 Å	4.9	7.5	6.9	8.4	3.3
9.5–5.5 Å	22.1	35.9	37.0	39.1	13.8
5.5–4.3 Å	47.9	63.8	64.3	68.4	33.2
4.3–4.0 Å	56.5	71.8	71.3	77.2	41.6

*Amplitude-weighted phase differences between independent half-data sets in successive resolution zones; random value, 90°.

based on the structure of AChBP (see Methods). The phases were significant to 4-Å resolution after the terms from many images of the same helical family had been added (Table 1). Structures were synthesized from the amplitude and phase terms in each family and combined, by averaging in real space, to obtain the final three-dimensional density map.

The real-space averaging brought about a substantial improvement in signal/noise ratio (Fourier shell correlation coefficient of 0.5 (refs 12, 13) at 4.0 Å; Supplementary Fig. 1), and enabled the polypeptide chains to be fitted to the densities (see Methods) after assigning the four helical segments as in ref. 8, with the beginning of M1 aligning with the carboxy-terminus of the corresponding portion in the ligand-binding domain. Figure 2 gives examples of the chains superimposed on the densities.

Interface with ligand-binding domain

Experiments with chimaeric molecules first showed that separate stretches of the amino-acid sequence are used to make the ligand-binding region and the membrane-spanning pore of ion channels in the ACh receptor superfamily[14]. In the structure, the interface between these two parts is marked by an abrupt transition from a predominantly β-sheet fold to an α-helical fold (Fig. 3a). Surprisingly, we find that this interface is not at the surface of the 30-Å-thick membrane (indicated in Fig. 1), but about 10 Å away. Thus the domain shaping the lumen of the pore is longer than is commonly assumed, with the α-helical segments, M1–M4, each continuing for some distance beyond the hydrophobic core of the membrane on the extracellular side.

Pentameric pore

The pore presents a tapering pathway for the ions when viewed from the synaptic cleft, and is encircled by a near-perfect five-fold arrangement of α-helical segments, in which each subunit resembles the blade of a propeller (Fig. 3b). The inner, pore-lining helices (M2) tilt radially inwards toward the central axis until they reach the middle of the membrane. In contrast, the outer helices (M1, M3 and M4) tilt both radially toward, and tangentially around, the central axis. This gives rise to a left-handed coiling, with M1 and M3 twisting together in a notably regular way (see also Supplementary Information movie).

The helices are splayed apart on the extracellular side of the membrane (centre-to-centre separation: 12.5–15 Å; Fig. 2a), and
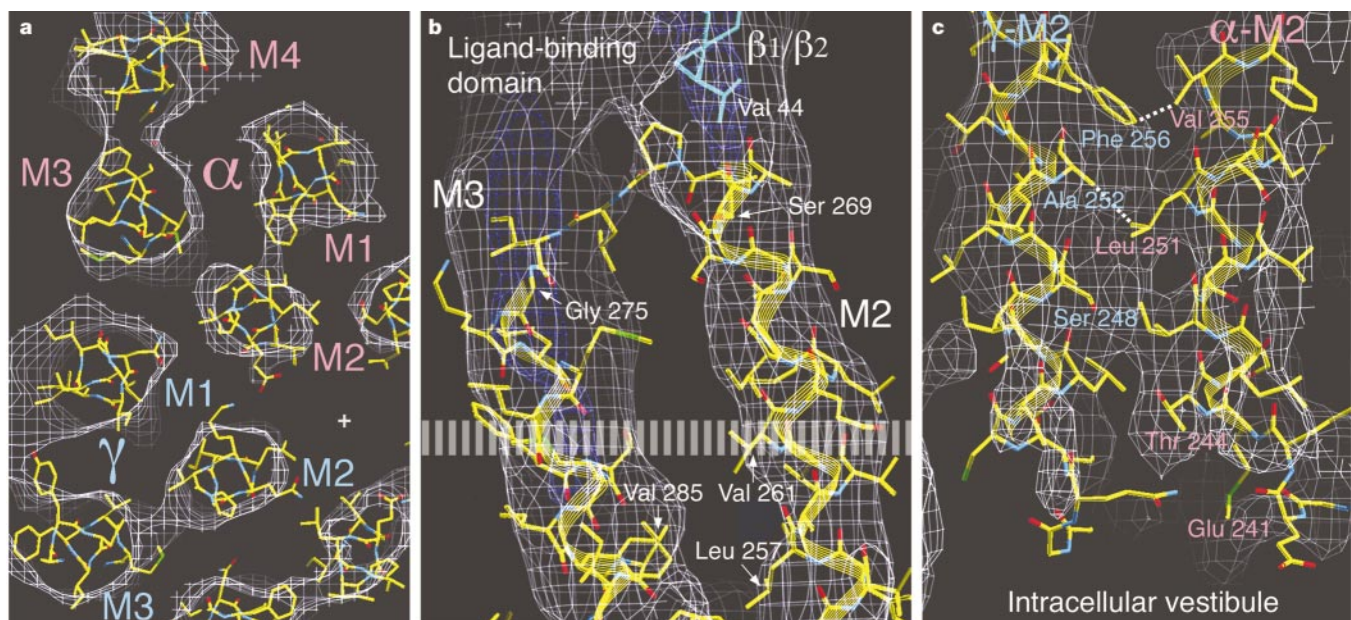

Figure 2 Representative portions of the polypeptide chains superimposed on the density map. **a**, Cross-section through the α-helices at the outer membrane surface; the cross denotes the pore axis; contours at 1.5σ. **b**, Longitudinal section through the M2, M3 helices, and the aligned β1/β2 loop (α-subunit); the broken line denotes the membrane surface; contours at 2σ (white) and 4σ (blue). **c**, Interaction between the α and γ M2 helices, viewed from the pore axis; putative hydrophobic contacts involving α-Leu 251 and α-Val 255 are indicated by dotted lines; the M2 helices end abruptly near α-Thr 244; contours at 2σ.

may possibly allow ions at the membrane surface to enter the pore laterally, bypassing the alternative route through the outer vestibule (Fig. 1). The largest openings are at the subunit interfaces, and extend into the ligand-binding domain (asterisk, Fig. 3a).

The sets of inner and of outer helices come together separately near the middle of the membrane, creating intervening spaces having dimensions comparable with those of the central hole (Fig. 3c). This suggests that there are just two essential structural components of the pore: an inner ring (blue) that interacts directly with the centrally passing ions, and an outer shell, or scaffold (red), that sequesters this ring away from the surrounding lipids. Such partitioning would be consistent with the findings of earlier experiments on the tubular crystals, which showed that the inner part moves when the receptor is activated, whereas the outer part remains unchanged[15].

It is notable that glycine and GABA$_A$ receptors, in the ACh receptor superfamily, have specific binding sites for alcohols and anaesthetics thought to be in water-filled cavities behind the inner (M2) helices[16]. The implicated amino acids are Ser 267 (glycine receptor) and Ser 270 (GABA$_A$ receptor) on the M2 segments of the α-subunits[17]. These residues align with α-Leu 257 (arrowhead, Fig. 3c), which faces the space between the inner and the outer sets of helices. Hence this space must be where the alcohols/anaesthetics bind in the other receptors.

Subunit topology and folding

Each subunit of the pore corresponds to a single protein domain, with maximum dimensions of ∼50 Å both normal to and parallel to the membrane plane. The domain consists of the four membrane-spanning helices, M1–M4, predicted by hydropathy plots, the extensions of these helices beyond the outer membrane surface, and connecting loops (Fig. 4a). The ends of the transmembrane portions of M1, M2 and M4 are framed by polar and/or negatively charged groups (at: α-Asn 217 and α-Asp 238; α-Glu 241 and α-Glu 262; α-Asp 407 and α-Gly 428).

The subunit fold is like that of the 'classical' 4-α-helical bundle found in myohemerythrin and tobacco mosaic virus, with the helices next to each other in the sequence being arranged in consecutive positions around the bundle (Fig. 4b). The group of helices, M1, M3 and M4, appears to be stabilized in the membrane by clustering of hydrophobic side chains around a central aromatic residue (α-Phe 233). Helix M2 makes no extensive van der Waals contacts with either M1 or M3, suggesting that it is mainly separated from these helices by water-filled space. There are, however, several close appositions between hydrophobic side chains on M2 and M3 (for example, Leu 250-Ile 296; Leu 257-Ile 289, and Val 261-Val 285 on the α-subunits) and on M2 and M1 (Leu 253-Phe 225). These (potential) interactions are likely to affect relative movements of the inner helices and outer shell of the pentamer during gating.

When individual subunits are aligned by bringing them into strict five-fold register, the helices M1, M2 and M3 superimpose well, especially over their membrane-spanning portions (r.m.s. variations in Cα positions: 0.53 Å (M2); 0.82 Å (M1); 1.04 Å (M3)). Helix M4 is less precisely positioned (r.m.s. variation: 1.74 Å), and comes away from the others, by variable amounts, at its extracellular end.
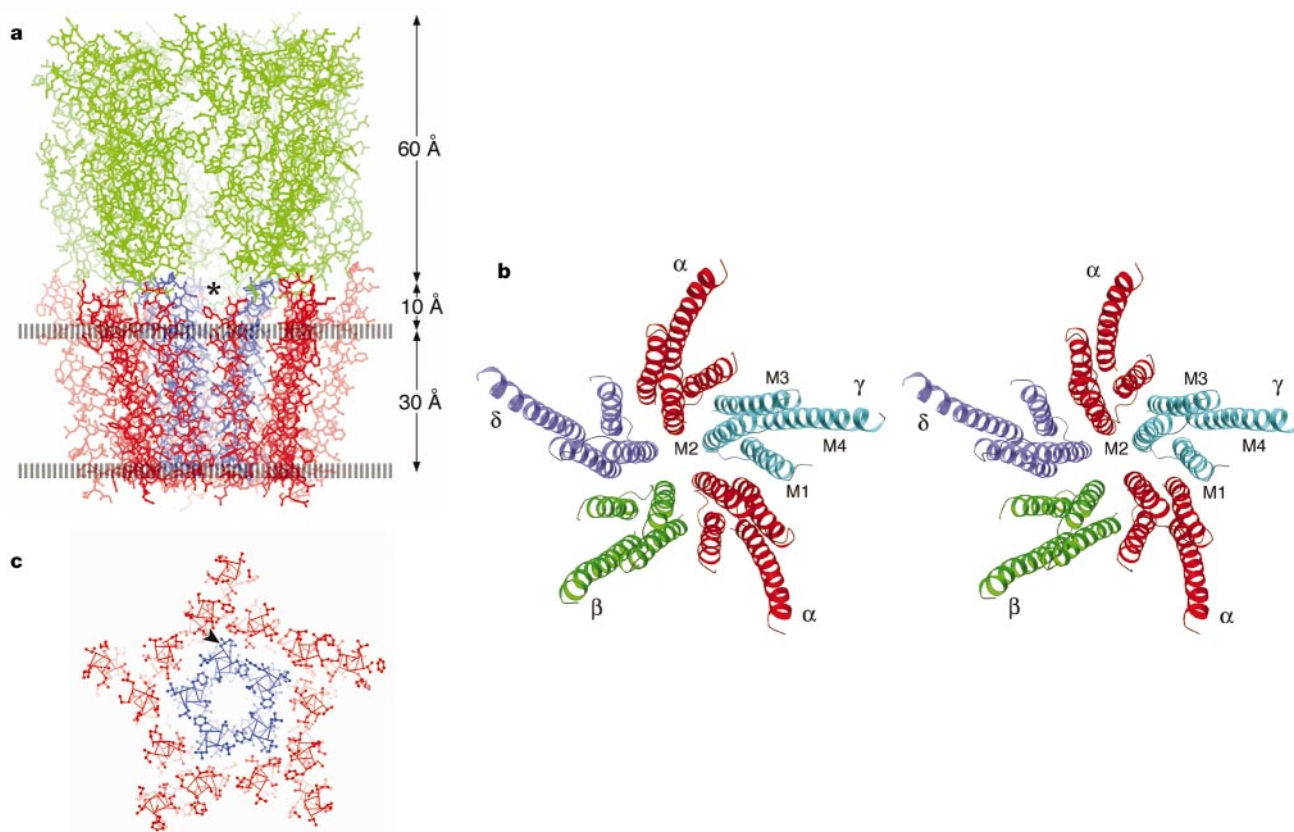

Figure 3 Pentameric structure of the pore. **a**, View normal to the receptor axis showing the α-helical pore structure (blue, pore-facing; red, lipid-facing helices) in relation to the membrane surfaces (broken lines) and the β-sheet structure (green) comprising the ligand-binding domain[8] (ball-and-stick representation); the asterisk denotes open space at a subunit interface. **b**, Stereo view of the pore, as seen from the synaptic cleft, with subunits shown in different colours (α, red; β, green; γ, cyan; δ, blue)[8]. **c**, Cross-sectional slab through the pentamer at the middle of the membrane, showing partitioning of the structure into pore- and lipid-facing parts, with intervening spaces (ball-and-stick representation); the arrowhead identifies α-Leu 257 (see text).

The division of the structure into lipid- and water-facing surfaces is in good agreement with the results of experiments in which specific residues have been labelled using either hydrophobic or hydrophilic probes. Several of the residues on M1, M3 and M4 facing the interior of the membrane have been labelled with lipophilic reagents that can be photoactivated[18,19] (red regions; Fig. 4c). Others that face the lumen of the pore, or are outside the membrane interior, have been identified by cysteine substitution and labelling with small water-soluble compounds[20,21] (blue regions; Fig. 4d). In addition, several of the identified water-accessible residues distributed over M2 lie between this helix and the others (α-Leu 250; α-Leu 258; the residues on the β-subunit aligning with α-257 and α-261 in Fig. 4a), consistent with the finding that M2 makes minimal contact with the outer shell of the pentamer (Figs 2b and 3c). Not surprisingly, some of the water-accessible residues on M2, and one on M1 (α-Leu 228)[18], have also been labelled by small hydrophobic reagents (green regions; Fig. 4d).

Ion conduction path

The M2 helices shaping the central conduction path are 40-Å long (including the portions outside the membrane), and are slightly kinked at α-Pro 265 and in the vicinity of α-Leu 251 (Fig. 5a). These helices traverse the membrane in register with sets of homologous residues at each level forming rings of chemically distinct environments facing the lumen of the pore[22,23] (Fig. 5b). The rings are predominantly non-polar, and would present a relatively inert surface to diffusing ions, but two of them (the rings at α-Ser 266 and at α-Glu 262) contain negatively charged groups, which would be expected to influence transport when the pore is open by raising the local cation concentration while lowering the concentration of anions. Mutation combined with electrophysiological experiments had drawn attention to the likely importance of these rings in affecting cation transport[24,25]. A third negatively charged ring shown to influence ion conduction, the 'intermediate ring' at α-Glu 241 (ref. 25), is in the loop region slightly beyond the ends of the M2 helices, and framing the intracellular entrance of the pore. Nearby
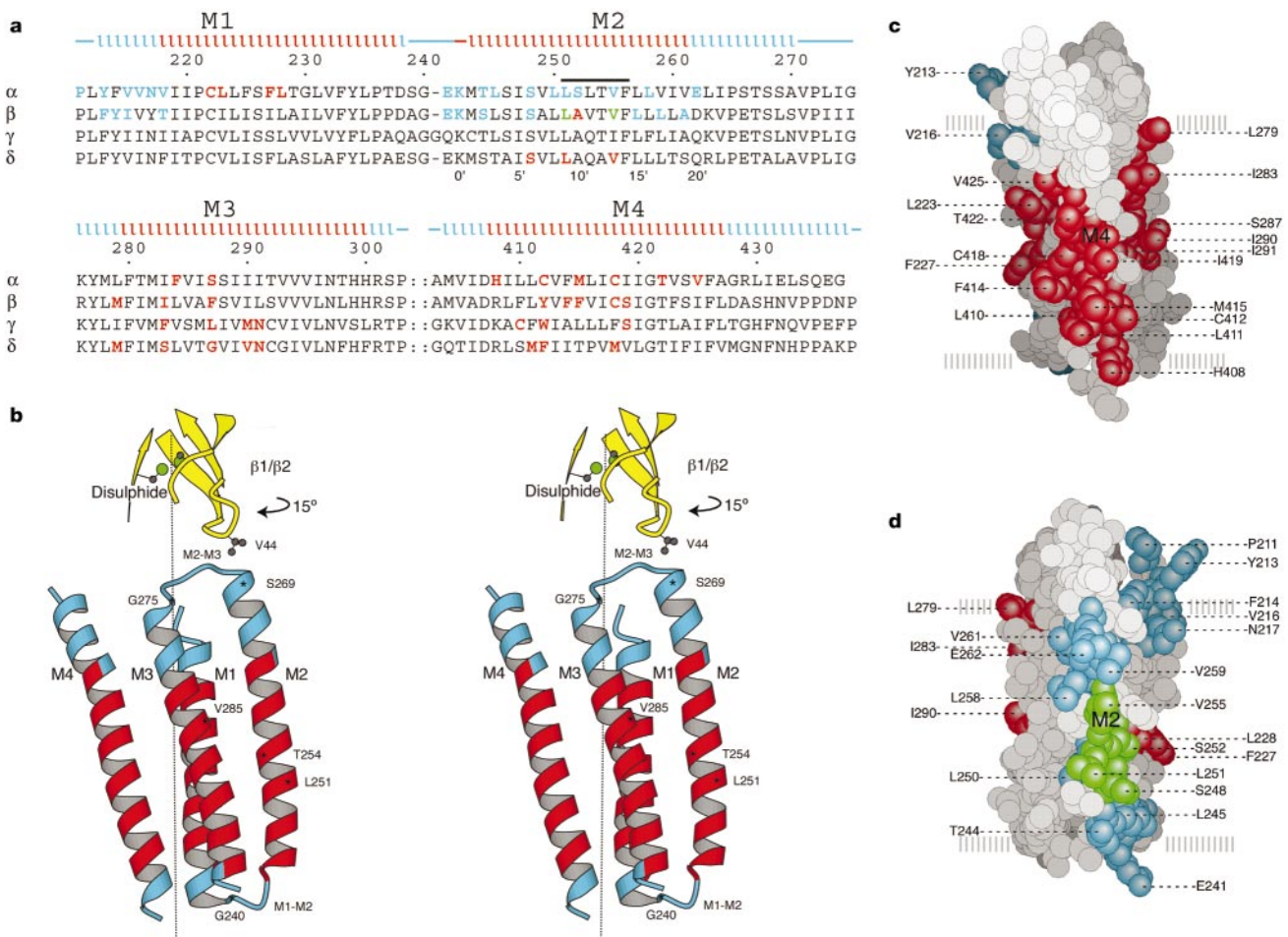

Figure 4 Overview of a pore-forming subunit. **a**, Amino-acid sequences (*Torpedo californica*) of the pore domain of the four aligned polypeptides (α-subunit numbering). The positions of the helical segments, M1–M4, and connecting loops (continuous lines) are indicated above the sequence (red, inside membrane; blue, outside membrane). The gate region on M2 is indicated by the black bar; residues along M2 are also identified according to the primed numbering system[26] (thus 9′ corresponds to α-Leu 251). Highlighted residues have been labelled with hydrophobic probes[18,19] (red), with hydrophilic methanethiosulphonate derivatives after substitution by cysteine[20,21] (blue), or with both (green). The extended loop between M3 and M4 is not shown. **b**, Stereo view of the subunit fold (α-subunit), as seen from the subunit interface, with portions inside and outside the membrane coloured respectively red and blue. The M2–M3 loop (α-Val

271–α-Gly 275) is resolved in all subunits; the M1–M2 loop (α-Ser 239–α-Lys 242) is less well defined, and the trace shown represents the most likely assignment. Also shown are the locations of the inner-sheet loop, β1/β2, and the 'cys-loop' disulphide bridge from the ligand-binding domain[8]. α-Val 44 in the β1/β2 loop docks into the hydrophobic pocket at the end of M2 (see Fig. 2b). The arrow denotes the 15° rotation of the β1/β2 loop about an axis through the disulphide bridge (vertical line) which leads to opening of the pore. **c**, **d**, Space-filling representations of the α-subunit, viewed from outside (**c**) and inside (**d**) the pore, showing the locations of the residues highlighted in **a** relative to the membrane surfaces (broken lines); residues in red, blue and green are labelled with hydrophobic probes, with hydrophilic probes, and with both, respectively (information from all subunits combined).
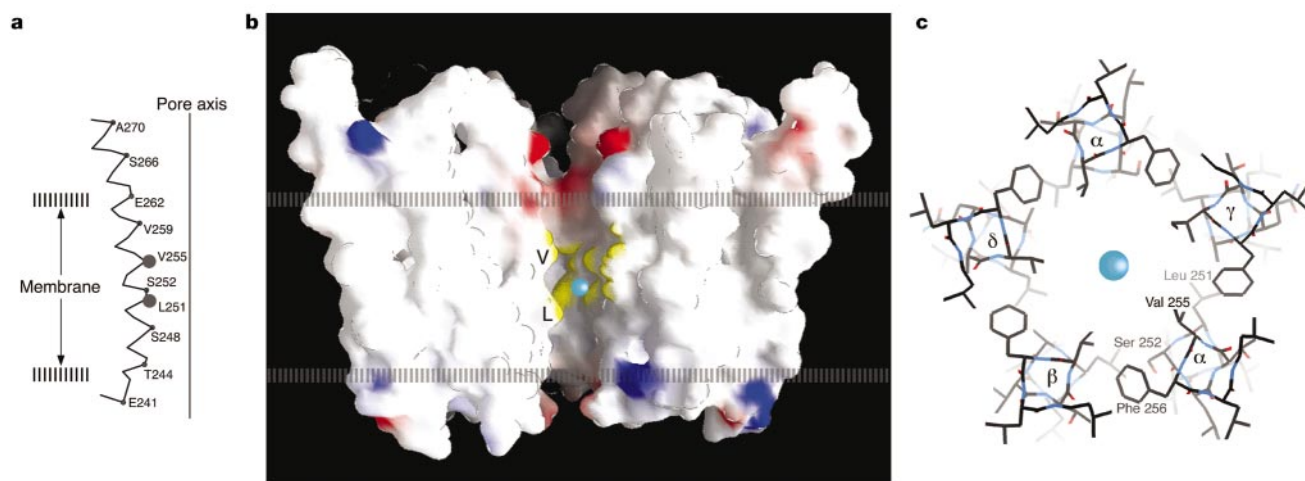
Figure 5 Lining of the pore. **a**, M2 helix showing locations of pore-facing side chains (α-subunit; Cα trace). **b**, Molecular surface of the pore domain with front subunit removed, rendered with GRASP[47]. Red and blue correspond respectively to areas of high negative and high positive charge; yellow highlights the hydrophobic area containing the gate; V and L identify α-Val 255 and α-Leu 251. **c**, Symmetrical arrangement of side chains forming the gate, as interpreted in Fig. 2c. The blue sphere in **b** and **c** is the size of a sodium ion (a hydrated ion may be trapped in this region).

small polar residues (at α-Thr 244, α-Ser 248, α-Ser 252), in the most constricting region of the open pore[26,27], are either partly or fully exposed to the ions.

The gate

The pore has special properties in the middle of the membrane. First, it is maximally constricted in this region, owing to the small separation of the M2 helices and to the presence of bulky hydrophobic side chains. Second, it is essentially symmetrical in this region, owing to equal side-to-side hydrophobic interactions between equivalent surfaces of homologous residues (Fig. 5c). The contacts are at two levels: one involving leucine (at α-Leu 251) with the neighbouring alanine (or serine) side chains (at α-Ser 252), and the other phenylalanine (at α-Phe 256) with the neighbouring valine (or isoleucine) side chains (at α-Val 255).

These symmetrical side-to-side interactions bring together the side chains on the neighbouring helices to make a tight hydrophobic girdle around the pore. The minimum radial distance from the central axis to the nearest van der Waals surface[28] is close to 3 Å at α-Leu 251 and at α-Val 255, where the pore is narrowest, and less than 3.5 Å over a ~8-Å-long hydrophobic zone extending to α-Val 259. This bore is too constricting for a sodium or potassium ion to pass through while retaining its first hydration shell (giving it an effective diameter of ~8 Å), and the ion cannot readily lose part of this shell in the absence of polar surfaces that would substitute for water. The girdle therefore creates an energetic barrier to ion permeation across the lipid bilayer[29]. It is the only such barrier along the conduction path, and there is no protein occlusion (for example, near the intracellular membrane surface[30]) that would block the flow of ions. Hence this region can be identified unambiguously as the gate of the pore.

The leucine (at α-251) and valine (at α-255) side chains contribute a major portion of the hydrophobic surface of the girdle, and their role as components of the gate is entirely consistent with the interpretation of photolabelling experiments using reagents that penetrate the lumen of the pore[19,31]. Residues in both rings are labelled efficiently by the small hydrophobic reagent, 3-(trifluoromethyl)-3-(m-[^{125}I]iodophenyl)diazirine[31], but only when the pore is closed and the side chains together form a compact hydrophobic binding environment. Moreover, in oocyte expression studies, mutation of the leucine to serine or threonine, in any of the subunits, increases the opening sensitivity of the channel[32,33]. This

would be expected, as perturbation of the hydrophobic contacts by the polar residues should weaken the girdle and increase the relative stability of the open pore.

Opening mechanism

The three-dimensional fold of the subunits in the ligand-binding domain is built around two sets of β-sheets packed into a curled β-sandwich and joined through a disulphide bridge[7]. By using the AChBP structure[7] as a template to relate maps derived from electron images, we showed that the two portions of the sandwich, in the α-subunits, convert to an alternative arrangement following activation by a 5-ms exposure to ACh[8]. This allosteric change to open the pore entails rotations of the inner (pore-facing) β-sheets by 15° about an axis passing through the disulphide bridge and oriented normal to the membrane plane[8].

The spatial relationship of the inner-sheet part of the α-subunit to the membrane-spanning domain was determined by rigid-body fitting of the inner-sheet part to the 4-Å densities (Fig. 2b; see also Methods). Figure 4b shows the two components in the region where they contact each other. The short loop joining the first two β-strands of the inner sheet (β1/β2; α-Glu 43–α-Gln 46; AChBP numbering) is positioned such that the end residue, α-Val 44, docks into the hydrophobic pocket made by the end residues (α-Ser 269–α-Pro 272) of the apposing M2 helix.

Although the limited resolution does not allow a full description, the pin-into-socket interaction between the β1/β2 loop and the end of M2 represents the sole direct link made between the moving elements in the two domains, both of which are found to rotate in the same sense when the receptor is activated[8,15]. The rotational movements of the inner sheets of the α-subunits are therefore necessarily communicated through this connection and along the pore-lining M2 helices to the gate at the middle of the membrane. For effective coupling, the M2 helices must be free to move relative to the outer protein wall. But this seems a likely possibility because the M2 helices only make limited contacts with the outer wall. Also, both connecting loops begin at conserved glycine residues (Gly 275 and Gly 240; Fig. 4b), lying near the rotation axis, which could confer flexibility by enabling rotational freedom around the peptide bond.

Electron microscopy had shown that the pore widens in the middle of the membrane when the receptor is activated[15]—that is, the hydrophobic girdle, forming the gate, comes apart to allow the
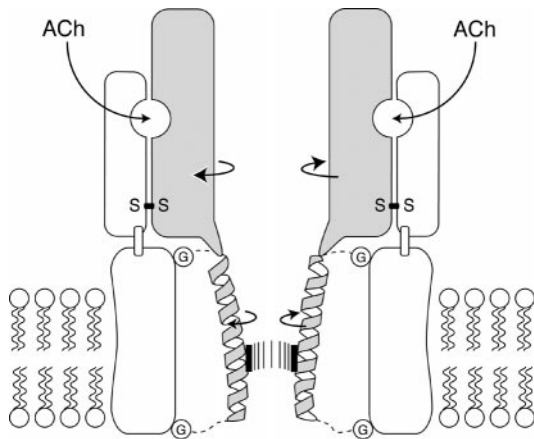
Figure 6 Proposed model for the gating mechanism. The ACh-induced rotations in the α-subunits[8] are transmitted to the gate—a hydrophobic barrier to ion permeation—through the M2 helices. The rotations destabilize the gate, causing the helices to adopt an alternative configuration which is permeable to the ions. The helices move freely during gating because they are mainly separated from the outer protein wall and connected to it by flexible loops, containing glycine residues (G). S-S is the disulphide-bridge pivot in the ligand-binding domain, which is anchored to the fixed outer shell of the pore. The relevant moving parts are shaded.

ions to flow through. How do the 15° rotational movements of the inner sheets of the α-subunits, communicated to the membrane-spanning domain, destabilize the girdle and open the pore? The structural details imply a simple mechanical model for the mechanism (Fig. 6). First, the allosteric change in the ligand-binding domain, which affects primarily the α-subunits, brings about the rotations of their inner sheets. Second, the rotations of the inner sheets are transmitted by their connected M2 helices to the girdle, or gate, at the middle of the membrane. Third, the twisting movement weakens the hydrophobic side-to-side interactions that hold the girdle together. As a result, the helices 'collapse' back against the outer protein wall, making alternative hydrophobic contacts in a configuration that is permeable to the ions.

The integrity of the girdle, like that of other symmetrical assemblies, may depend on equal interactions between each of its components. Thus when only one of these components is sufficiently perturbed, the neighbouring component will lose a set of interactions maintaining its position in the assembly, setting in train cooperative changes that cause the whole structure to flip. The action of just two ligand-binding subunits transmitted to a symmetrical pore may well represent an optimal way to achieve fast and robust gating kinetics, while minimizing the number of activating molecules.

Discussion

The structure of the pore, and our picture of the working protein, are in excellent agreement with the results obtained from several well characterized mutations. Mutations in the pore domain that would affect gating can be divided into three categories: (1) those that influence the coupling between the M2 helices and the ligand-binding domain; (2) those that influence the side-to-side interactions between the M2 helices; and (3) those in other regions that interfere with their movements. An example in category (1) would be the natural mutation of α-Ser269Ile, at the end of M2 next to the inner sheet of the ligand-binding domain (Fig. 4b). This mutation is the cause of a congenital myasthenic syndrome (CMS), and prolongs the apparent open-channel lifetime[34,35]. However, the lifetime is not altered by the same mutation at equivalent positions in any of the three non-α-subunits[35], consistent with the special role played by the α-subunits in transmitting the conformational

change. ε-Thr264Pro is another CMS mutant, which gives rise to spontaneous and prolonged channel openings[36]. It is an example in category (2), because the residue (aligning with α-Thr 254; Fig. 4b) is a component of the girdle, or gate. The introduction of the helix-bending proline at the gate would be expected to weaken it and shift the equilibrium in favour of open events. The CMS mutation α-Val285Ile, which leads to abnormally brief channel openings[37], is an example in category (3). α-Val 285 is on the M3 helix close to α-Val 261 on M2 (Fig. 2b), and the larger isoleucine side chain in this position could facilitate interaction between the non-moving (M3) and moving (M2) parts, consistent with the interpretation that the mutant stereochemically inhibits the gating movements[37]. Finally, several experiments have highlighted the uniqueness of the girdle-stabilizing leucine residue (at α-Leu 251) in relation to the gating mechanism. One observation is that replacement of the leucine by serine increases the opening sensitivity of the channel by the same amount, independent of which subunit is mutated[32]. This property supports the idea that symmetry is important in determining the integrity of the gate.

Our results from electron images have yielded the first detailed information about the fold and arrangement of the protein chains forming the pore of a transmitter-gated ion channel. They clarify the nature of the gate in the ACh receptor, and suggest how ACh entering the ligand-binding domain triggers pore opening. It is possible that other neuronal ion channels make use of the same physical principles to achieve precise control of ion flux across the lipid bilayer. □

Methods

Specimen preparation and imaging

Tubular crystals were grown from the postsynaptic membranes of *Torpedo marmorata* electric organ in 100 mM sodium cacodylate, 1 mM calcium chloride, pH 6.8, using fish killed in the autumn[38]. They were applied to pre-irradiated holey carbon grids, having high electrical conductivity, and frozen rapidly by plunging into liquid-nitrogen-cooled ethane. Images were recorded at 4 K in ice over holes, using a 300-kV field emission microscope incorporating a top-entry liquid-helium-cooled stage[10] (magnification, ×36,800; defocus range, 9,000–16,000 Å; dose, ~20 electrons Å^{-2}).

ACh receptor tubes are helical assemblies of protein and lipid molecules arranged on a *p*2 surface lattice[6]. We examined four helical families ((−16,6); (−18,6); (−17,5); (−15,7)), with diameters ranging from 770 to 832 Å (Table 1).

Analysis of images

The basic methods for selecting and analysing the images in terms of helical Fourier transforms have been described[11,38,48]. At higher resolution in the equatorial direction, many of the layer-lines overlap and interfere with one another. But different tubes give rise to different patterns of overlap, because of slight variations in orientation of the surface lattice, and the interference error is largely averaged out after many images have been combined[38]. Altogether 72 unique overlap patterns, within the four helical families, were identified and analysed. Correction for Ewald sphere curvature was calculated from the helical geometry[39].

The tubes contain various distortions that give rise to serious loss of signal at resolutions higher than ~10 Å. We corrected for the distortions by dividing the tubes into short segments, fitting successive segments independently to a reference structure, and then adding the segments to the reference data set after the misalignments had been removed[11]. The reference data set, for each helical family, was thus updated in a cumulative way. In this study the improved reference structure, resulting from addition of many images, allowed the segment length to be shortened to a mean value of 679 Å (compared with 759 Å previously[38]; see Table 1), without increasing the alignment error, thus improving the accuracy of the correction procedure.

To obtain an appropriate scaling for the amplitudes, we compared the experimental measurements with calculated values, using a model tube having the receptor replaced by just the ligand-binding domain in one case, and by the AChBP structure[7] in the other. To determine the helical transform of the ligand-binding domain, we calculated the helical density waves, $g(n,r)$, by Fourier–Bessel inversion of the layer-line data[40,41], and then back-transformed using only those $g(n,r)$ terms lying within the relevant radial range (indicated by the green box in Fig. 1). The helical transform of AChBP, in the equivalent lattice positions, was calculated from the AChBP coordinates (1I9B from the Protein Data Bank), using a program written by M. Stowell. Plots of the ratios of the amplitudes in the two Fourier transforms, at equivalent points along the layer-lines, indicated there were two components to the resolution-dependent loss of signal from the receptor: a pronounced fall-off at low resolution, and a more gradual 'fade-out' at higher resolution (Supplementary Fig. 2). These effects could be attributed, respectively, to the presence of a proportion of receptors that were not properly ordered on the surface lattice and to imaging deficiencies, such as beam-induced movement and radiation damage[42]. Similar resolution-dependent fall-offs were observed with all helical families. The loss of signal in

each case was compensated by subtracting the low-resolution structure ($<1/15\,\text{Å}^{-1}$; 84% weight), and sharpening by a temperature factor of $-110\,\text{Å}^2$ to restore an approximately constant amplitude ratio over the whole resolution range. The rescaling of the amplitude terms was critical in improving the definition of the outermost membrane-spanning α-helices (Supplementary Fig. 3), which were 'swamped out' by the low resolution terms in studies[9,15] where this correction was not applied.

Structure determination and evaluation

Structures were calculated from each of the four helical families, in the standard way[41], using all significant Fourier terms extending to 4 Å (corresponding to the cut-off angle made by the objective aperture in the microscope). To evaluate the reliability and resolution of the three-dimensional maps, we first divided the data sets of each family into two halves and calculated maps from these halves. Single molecules isolated from the maps were then compared to determine amplitude-weighted phase differences and Fourier shell correlation coefficients in successive annuli of increasing resolution (Table 1; Supplementary Fig. 1). The final density map was a weighted average of the four aligned structures, as before[38], but with each of the structures being derived from about twice as many images.

The cosine of the phase error in Table 1 gives a measure of the quality of the calculated structures. We find that this parameter, near the resolution limit, is approximately proportional to the square root of the number of receptors averaged, irrespective of the helical family or whether different families have been combined (Supplementary Fig. 4). Our results are therefore limited primarily by the number of receptors averaged, and further studies should benefit from the implementation of automatic methods of data collection and analysis.

Interpretation of the final experimental density map and model building into the densities were performed using the program O[43]. Initially, we applied five-fold averaging to improve the definition of the α-helical backbone structures, and to establish the precise register and orientation of individual (polyalanine) helices. Subsequently, we fitted the M1–M4 helical segments individually to the experimental map, using the protruding regions along the helical densities to identify the largest side chains. This allowed tentative assignments to be made of each amino acid according to the sequence, both along the helices and along the short M2–M3 connecting loops. These assignments were then validated for each subunit by checking their consistency with residues in equivalent locations around the pentamer. PROCHECK[44] was used to assess and improve the stereochemical correctness of the initial hand-built atomic model, which has not been refined. Rigid body fitting to the densities of the inner sheet of the β-sandwich was done using the real-space refinement in O, and confirmed previous results[8] (where the estimated alignment error was $\pm0.9\,\text{Å}$). Figures were prepared with MOLSCRIPT[45], SETOR[46] and GRASP[47].

1. Hille, B. *Ion Channels of Excitable Membranes* (Sinauer Associates, Sunderland, Massachusetts, 2001).
2. Karlin, A. Emerging structure of the nicotinic acetylcholine receptors. *Nature Rev. Neurosci.* **3,** 102–114 (2002).
3. Corringer, J.-P., Le Novère, N. & Changeux, J.-P. Nicotinic receptors at the amino acid level. *Annu. Rev. Pharmacol. Toxicol.* **40,** 431–458 (2000).
4. Colquhoun, D., Shelly, C., Hatton, C., Unwin, N. & Sivilotti, L. Nicotinic acetylcholine receptors. *Burger's Med. Chem. Drug Discov.* **2,** 357–406 (2003).
5. Heuser, J. E. & Salpeter, S. R. Organization of acetylcholine receptors in quick-frozen, deep-etched and rotary-replicated *Torpedo* postsynaptic membrane. *J. Cell Biol.* **82,** 150–173 (1979).
6. Brisson, A. & Unwin, P. N. T. Tubular crystals of acetylcholine receptor. *J. Cell Biol.* **99,** 1202–1211 (1984).
7. Brejc, K. *et al.* Crystal structure of an ACh-binding protein reveals the ligand-binding domain of nicotinic receptors. *Nature* **411,** 269–276 (2001).
8. Unwin, N., Miyazawa, A., Li, J. & Fujiyoshi, Y. Activation of the nicotinic acetylcholine receptor involves a switch in conformation of the α subunits. *J. Mol. Biol.* **319,** 1165–1176 (2002).
9. Unwin, N. Nicotinic acetylcholine receptor at 9 Å resolution. *J. Mol. Biol.* **229,** 1101–1124 (1993).
10. Fujiyoshi, Y. *et al.* Development of a superfluid helium stage for high-resolution electron microscopy. *Ultramicroscopy* **38,** 241–251 (1991).
11. Beroukhim, R. & Unwin, N. Distortion correction of tubular crystals: Improvements in the acetylcholine receptor structure. *Ultramicroscopy* **70,** 57–81 (1997).
12. Van Heel, M. Similarity measures between images. *Ultramicroscopy* **21,** 95–100 (1987).
13. Bottcher, B., Wynne, S. A. & Crowther, R. A. Determination of the fold of the core protein of hepatitis B virus by electron cryomicroscopy. *Nature* **386,** 88–91 (1997).
14. Eisele, J.-L. *et al.* Chimaeric nicotinic-serotonergic receptor combines distinct ligand binding and channel specificities. *Nature* **366,** 479–483 (1993).
15. Unwin, N. Acetylcholine receptor channel imaged in the open state. *Nature* **373,** 37–43 (1995).
16. Wick, M. J. *et al.* Mutations of γ-aminobutyric acid and glycine receptors change alcohol cutoff: Evidence for an alcohol receptor? *Proc. Natl Acad. Sci. USA* **95,** 6504–6509 (1998).
17. Mascia, M. P., Trudell, J. R. & Harris, R. A. Specific binding sites for alcohols and anesthetics on ligand-gated ion channels. *Proc. Natl Acad. Sci. USA* **97,** 9305–9310 (2000).
18. Blanton, M. P. & Cohen, J. B. Identifying the protein-lipid interface of the *Torpedo* nicotinic acetylcholine receptor: Secondary structure implications. *Biochemistry* **33,** 2859–3872 (1994).
19. Blanton, M. P., Dangott, L. J., Raja, S. K., Lala, A. K. & Cohen, J. B. Probing the structure of the nicotinic acetylcholine receptor ion channel with the uncharged photoactivatable compound [³H]diazofluorene. *J. Biol. Chem.* **273,** 8659–8668 (1998).
20. Akabas, M. H., Kaufmann, C., Archdeacon, P. & Karlin, A. Identification of acetylcholine receptor channel-lining residues in the entire M2 segment of the α subunit. *Neuron* **13,** 919–927 (1994).
21. Zhang, H. & Karlin, A. Contribution of the β subunit M2 segment to the ion-conducting pathway of the acetylcholine receptor. *Biochemistry* **37,** 7952–7964 (1998).
22. Giraudat, J., Dennis, M., Heidmann, T., Chang, J. Y. & Changeux, J.-P. Structure of the high affinity binding site for noncompetitive blockers of the acetylcholine receptor: Serine-262 of the δ subunit is labelled by [³H]chlorpromazine. *Proc. Natl Acad. Sci. USA* **83,** 2719–2723 (1986).
23. Hucho, F. L., Oberthur, W. & Lottspeich, F. The ion channel of the nicotinic acetylcholine receptor is formed by the homologous helices MII of the receptor subunits. *FEBS Lett.* **205,** 137–142 (1986).
24. Imoto, K. *et al.* Location of a δ-subunit region determining ion transport through the acetylcholine receptor channel. *Nature* **324,** 670–674 (1986).
25. Imoto, K. *et al.* Rings of negatively charged amino acids determine the acetylcholine receptor channel conductance. *Nature* **335,** 645–648 (1988).
26. Charnet, P. *et al.* An open-channel blocker interacts with adjacent turns of α-helices in the nicotinic acetylcholine receptor. *Neuron* **2,** 87–95 (1990).
27. Villarroel, A., Herlitze, S., Koenen, M. & Sakmann, B. Location of a threonine residue in the α-subunit M2 transmembrane segment that determines the ion flow through the acetylcholine receptor channel. *Proc. R. Soc. Lond. B* **243,** 69–74 (1991).
28. Smart, O. S., Goodfellow, J. M. & Wallace, B. A. The pore dimensions of gramicidin A. *Biophys. J.* **65,** 2455–2460 (1993).
29. Beckstein, O., Biggin, P. C. & Sansom, M. S. P. A hydrophobic gating mechanism for nanopores. *J. Phys. Chem. B* **105,** 12902–12905 (2001).
30. Wilson, G. G. & Karlin, A. The location of the gate in the acetylcholine receptor channel. *Neuron* **20,** 1269–1281 (1998).
31. White, B. H. & Cohen, J. B. Agonist-induced changes in the structure of the acetylcholine receptor M2 regions revealed by photoincorporation of an uncharged nicotinic noncompetitive antagonist. *J. Biol. Chem.* **267,** 15770–15783 (1992).
32. Labarca, C. *et al.* Channel gating governed symmetrically by conserved leucine residues in the M2 domain of nicotinic receptors. *Nature* **376,** 514–516 (1995).
33. Filatov, G. N. & White, M. M. The role of conserved leucines in the M2 domain of the acetylcholine receptor in gating. *Mol. Pharmacol.* **48,** 379–384 (1995).
34. Croxen, R. *et al.* Mutations in different functional domains of the human muscle acetylcholine receptor α subunit in patient with the slow-channel congenital myasthenic syndrome. *Hum. Mol. Genet.* **6,** 767–774 (1997).
35. Grosman, C., Salamone, F. N., Sine, S. M. & Auerbach, A. The extracellular linker of muscle acetylcholine receptor channels is a gating control element. *J. Gen. Physiol.* **116,** 327–340 (2000).
36. Ohno, K. *et al.* Congenital myasthenic syndrome caused by prolonged acetylcholine receptor channel openings due to a mutation in the M2 domain of the ε subunit. *Proc. Natl Acad. Sci. USA* **92,** 758–762 (1995).
37. Wang, H.-L. *et al.* Acetylcholine receptor M3 domain: Stereochemical and volume contributions to channel gating. *Nature Neurosci.* **2,** 226–233 (1999).
38. Miyazawa, A., Fujiyoshi, Y., Stowell, M. & Unwin, N. Nicotinic acetylcholine receptor at 4.6 Å resolution: Transverse tunnels in the channel wall. *J. Mol. Biol.* **288,** 765–786 (1999).
39. DeRosier, D. J. Correction of high-resolution data for curvature of the Ewald sphere. *Ultramicroscopy* **81,** 83–98 (2000).
40. Klug, A., Crick, F. H. C. & Wykoff, H. W. Diffraction by helical structures. *Acta Crystallogr.* **11,** 199–213 (1958).
41. DeRosier, D. J. & Moore, P. B. Reconstruction of three-dimensional images from electron micrographs of structures with helical symmetry. *J. Mol. Biol.* **52,** 355–369 (1970).
42. Henderson, R. Image contrast in high-resolution electron microscopy of biological materials. *Ultramicroscopy* **46,** 1–18 (1992).
43. Jones, T. A., Zou, J.-Y., Cowan, S. W. & Kjeldgaard, M. Improved methods for building protein models in electron density maps and the location of errors in these models. *Acta Crystallogr. A* **47,** 110–119 (1991).
44. Laskowski, R. A., MacArthur, M. W., Moss, D. S. & Thornton, J. M. PROCHECK: A program to check the stereochemical quality of protein structures. *J. Appl. Crystallogr.* **26,** 283–291 (1993).
45. Kraulis, P. J. MOLSCRIPT: A program to produce both detailed and schematic plots of protein structures. *J. Appl. Crystallogr.* **24,** 946–950 (1991).
46. Evans, S. V. SETOR: Hardware lighted three-dimensional solid model representations of macromolecules. *J. Mol. Graph.* **11,** 134–138 (1993).
47. Nicholls, A., Sharp, K. & Honig, B. A rapid finite difference algorithm, utilizing successive over-relaxation to solve the Poisson-Boltzmann equation. *J. Comput. Chem.* **12,** 435–445 (1991).
48. Toyoshima, C. & Unwin, N. Ion channel of acetylcholine receptor reconstructed from images of postsynaptic membranes. *Nature* **336,** 247–250 (1988).